Available on CMS information server

**CMS CR -2019/307**

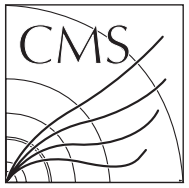

**The Compact Muon Solenoid Experiment**

# Conference Report

Mailing address: CMS CERN, CH-1211 GENEVA 23, Switzerland

**19 December 2019 (v4, 13 May 2020)**

# Performances of highly irradiated 3D and planar pixel sensors interconnected to the RD53A readout chip

R. Ceccarelli, A. Cassese, M. Meschini, L.Viliani, M. Dinardo, S. Gennai, L. Moroni, D.Zuolo, A. Messineo, G.F. Dalla Betta, M. Boscardin on behalf of the CMS Tracker Group

**Abstract**

The High Luminosity upgrade of the CERN Large Hadron Collider (HL-LHC) calls for new highly radiation tolerant silicon pixel sensors, capable of withstanding fluences up to $2.3 \times 10^{16}\,\mathrm{n_{eq}/cm^2}$ (1 MeV equivalent neutrons). In this paper results obtained in beam test experiments with 3D and planar pixel sensors interconnected with the RD53A readout chip are reported. RD53A is the first prototype in 65 nm technology issued by the RD53 collaboration for the future readout chip to be used in the upgraded pixel detectors. The interconnected modules have been tested in a proton beam at CERN or an electron beam at DESY, before and after irradiation, which was performed at the CERN IRRAD facility or at the KIT Irradiation Center, up to an equivalent fluence of $1 \times 10^{16}\,\mathrm{n_{eq}/cm^2}$. The sensors were made by FBK foundry in Trento, Italy, and their development was done in collaboration with INFN (Istituto Nazionale di Fisica Nucleare, Italy). The analysis of the collected data shows hit detection efficiencies around 99% measured after irradiation. All results are obtained in the framework of the CMS R&D activities.

Presented at *IPRD2019 15th Topical Seminar on Innovative Particle and Radiation Detectors*

Journal of Instrumentation

# Performances of highly irradiated 3d and planar pixel sensors interconnected to the RD53A readout chip



Published by IOP Publishing for Sissa Medialab

Received: *December 29, 2019*
Accepted: *January 10, 2020*
Published: *February 11, 2020*

15th Topical Seminar on Innovative Particle and Radiation Detectors
14–17 October 2019
Siena, Italy

# Performances of highly irradiated 3d and planar pixel sensors interconnected to the RD53A readout chip

**A. Cassese,[a] R. Ceccarelli,[a,1] M. Meschini,[a] L. Viliani,[a] M. Dinardo,[b] S. Gennai,[b] L. Moroni,[b] D. Zuolo,[b] A. Messineo,[c] G.F. Dalla Betta[d] and M. Boscardin[e]**
**on behalf of the CMS Tracker Group**

[a] *INFN Firenze, via Sansone 1, Sesto Fiorentino, Firenze, Italy*
[b] *INFN and University of Milano Bicocca and Physics Department, University of Milano Bicocca, Piazza della Scienza 3, Milano, Italy*
[c] *INFN and Physics Department, University of Pisa, Largo B. Pontecorvo 3, Pisa, Italy*
[d] *TIFPA INFN and Department of Industrial Engineering, University of Trento, Via Sommarive 9, Trento, Italy*
[e] *Fondazione Bruno Kessler, Centro Materiali e Microsistemi (FBK-CMM), 38123 Povo di Trento, Trento, Italy*

*E-mail:* rudy.ceccarelli@fi.infn.it

Abstract: The High Luminosity upgrade of the CERN Large Hadron Collider (HL-LHC) calls for new highly radiation tolerant silicon pixel sensors, capable of withstanding fluences up to $2.3 \times 10^{16}\,n_{eq}/cm^2$ (1 MeV equivalent neutrons). In this paper results obtained in beam test experiments with 3D and planar pixel sensors interconnected with the RD53A readout chip are reported. RD53A is the first prototype in 65 nm technology issued by the RD53 collaboration for the future readout chip to be used in the upgraded pixel detectors. The interconnected modules have been tested in an electron beam at DESY, before and after irradiation, which was performed at the CERN IRRAD facility for the 3D sensors or at the KIT Irradiation Center for the planar sensors, up to an equivalent fluence of $1 \times 10^{16}\,n_{eq}/cm^2$. The sensors were made by FBK foundry in Trento, Italy, and their development was done in collaboration with INFN (Istituto Nazionale di Fisica Nucleare, Italy). The analysis of the collected data shows hit detection efficiencies around 99% measured after irradiation. All results are obtained in the framework of the CMS R&D activities.

Keywords: Performance of High Energy Physics Detectors; Radiation damage to detector materials (solid state); Radiation-hard detectors; Radiation-hard electronics

[1] Corresponding author.


https://doi.org/10.1088/1748-0221/15/02/C02016

2020 JINST 15 C02016

## Contents



2020 JINST 15 C02016

## 1 Pixel sensors for HL-LHC

Pixel detectors in the innermost layers of the High Luminosity Large Hadron Collider (HL-LHC) experiments will have to withstand a fluence that can exceed $2 \times 10^{16}\,n_{eq}/cm^2$, while preserving high tracking efficiency [1].

Two different technological solutions are available: planar sensors, where the electrodes are parallel to the sensor surface, and 3D sensors, where the electrodes are orthogonal to the sensor surface. In the first case the distance between the electrodes is fixed by the sensor's active thickness, in the second case the distance between electrode is usually shorter than the full active thickness and it is determined according to the layout and the technological process chosen to build the sensor. To keep the pixel occupancy at the 0.1% level at the conditions expected at HL-LHC, and to have a good spatial resolution, two pixel cell sizes are under study: $50 \times 50\,\mu m^2$ and $25 \times 100\,\mu m^2$. The total active sensor thickness will be between 100 and 150 µm in order to keep both the bias voltage and the power dissipation after irradiation at a manageable level, while at the same time allowing for a reasonable amount of collected charge to reach full hit detection efficiency. The radiation damage reduces the effective drift distance of charge carriers because of charge trapping, so it is not useful, in the case of planar sensors, to increase the thickness beyond the above limits. 3D pixel sensors, where charge carriers have to travel distances much shorter than the sensor thickness (only 35 µm for a $50 \times 50\,\mu m^2$ pixel pitch independently of the sensor thickness, which is the driving parameter for planar pixel sensors), are hence very good candidates to satisfy all of the above requirements.

## 2 Tested sensors and irradiations

In February and April 2019 we tested on beam two planar pixel sensors and one 3D pixel sensor.

The two planar pixel sensors were fabricated at the FBK foundry in Trento and were developed within a collaboration program with INFN (Istituto Nazionale di Fisica Nucleare, Italy). The substrates selected are p-type Si-Si Direct Wafer Bond (DWB). The handle wafer is 500 µm thick low resistivity Czochralski silicon. FBK active devices are implanted on a Float Zone (FZ), high

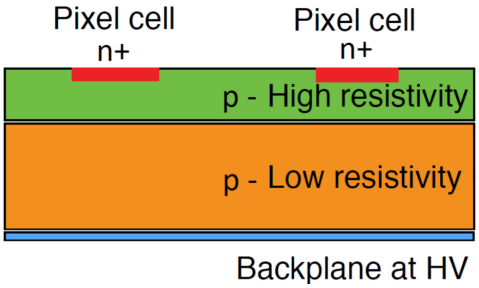


**Figure 1.** Sketch of the cross section of a FBK planar sensor.

resistivity (> 3000 Ohm cm), 100 µm thick wafer. A temporary metal layer is used for sensor testing at FBK premises and is subsequently removed. In one of the tested planar sensors, the pixels are equipped with an additional $n^+$ implant, the bias punch-through structure, placed at the intersection of a $2 \times 2$ pixel grid, which is also used for sensor testing at FBK premises. The presence of this implant may affect efficiency, as described in this paper. In figure 1 a sketch of the cross section of an FBK planar sensor is shown.

The tested 3D pixel sensor was fabricated at FBK and developed in the same collaboration program as the planar pixel sensors [2]. The same DWB technique was used, but in this case the active thickness of the FZ silicon was 130 µm. Columnar electrodes of both $p^+$ and $n^+$ type are etched by Deep Reactive Ion Etching (DRIE) in the wafer using a top-side only process. In figure 2 a sketch of the cross section of an FBK 3D sensor is shown.

After fabrication pixel sensor wafers (both planar and 3D) were processed for UBM (Under Bump Metalization), thinned, diced and bump-bonded to RD53A prototype readout chips [3] at IZM (Berlin, Germany). The RD53A chip has 76800 readout channels (400 rows and 192 columns with a bump pad pitch of $50 \times 50\,\mu m^2$ ) and measures $20.1 \times 11.6\,mm^2$. RD53A contains three front-ends, named Synchronous, Linear and Differential, to allow performance comparisons between different analog designs. All results presented here were obtained with the Linear front-end, placed in the central zone of RD53A (136 columns wide, from 128 to 263).

The pixel sensor bonded to the readout chip needs to be glued and wire-bonded onto a light PCB card that can be connected to an adapter card in order to be tested; these units will be referred to as pixel modules in the following. The PCB card was designed in order to withstand significant irradiation without activating.

The two planar modules were irradiated at KIT Irradiation Centre in a 23 MeV proton beam, to an estimated fluence of $0.5 \times 10^{16}\,n_{eq}/cm^2$, corresponding to a total ionizing dose of about 7.2 MGy. The 3D module was irradiated at the CERN IRRAD facility in 2018 in a high intensity 24 GeV proton beam (which has a FWHM of 12 mm in $x$ and $y$ directions), to an estimated fluence of $1 \times 10^{16}\,n_{eq}/cm^2$. The module was tilted with respect to the beam at an angle of 55° in order to achieve a more uniform irradiation.

## 3 The DESY Test Beam

The pixel modules were tested at the DESY Test Beam Facility, in the TB21 area. The DESY II synchrotron circulates one electron bunch at a frequency of about 1 MHz with a maximum energy of



2020 JINST 15 C02016

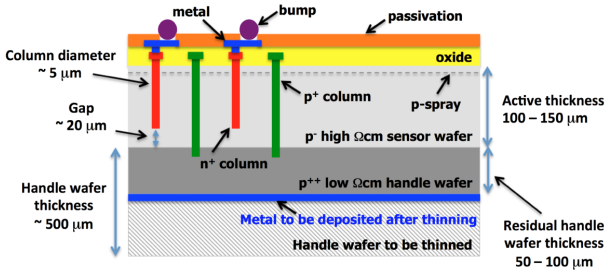


**Figure 2.** Sketch of the cross section of a FBK 3D sensor.

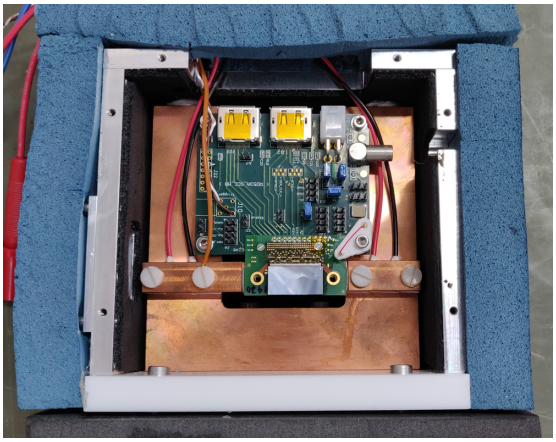

**Figure 3.** Tested module connected to the readout card and mounted inside the cooling box.

about 6.3 GeV. The beam is generated via a twofold conversion and a spectrometer dipole magnet enables momentum selection in the range of 1–6 GeV. The beam has a divergence of about 1 mrad and an energy spread of approximately 5%.

The test beam area is equipped with an EUDET-type pixel beam telescope (called DATURA) which allows to track the beam particles [4]. The telescope is composed of two arms, each made of three planes. The Device Under Test (DUT) is placed between the two arms, called upstream and downstream with respect to the beam direction. Each plane consists of a MIMOSA26 monolithic active pixel silicon sensor: the pixel size is 18.4 μm × 18.4 μm while the active thickness is 50 μm. Two scintillators are placed in front of the first telescope plane, forming a trigger window of approximately 10 mm × 10 mm. Moreover, a CMS Phase-1 pixel module is placed in front of the scintillators and is used as a timing reference.

The irradiated modules were kept inside a cooling box,[1] in order to keep them at a low and constant temperature. Inside the box, the downstream face of the DUT was in contact, through a thermally conductive paste, to a thin copper bar, which was kept cold (at about −27°C) by two Peltier cells, cooled by an external chiller. In figure 3 a photo of one of the tested modules, connected to the readout card and mounted in the cooling box, is shown.

The cooling box could be rotated, in order to acquire data for tracks inclined with respect to the DUT. We acquired data always requiring a 5.2 GeV electron beam.

[1]The cooling box is made of aluminium, but features an entry window for the incoming electron beam.



2020 JINST 15 C02016

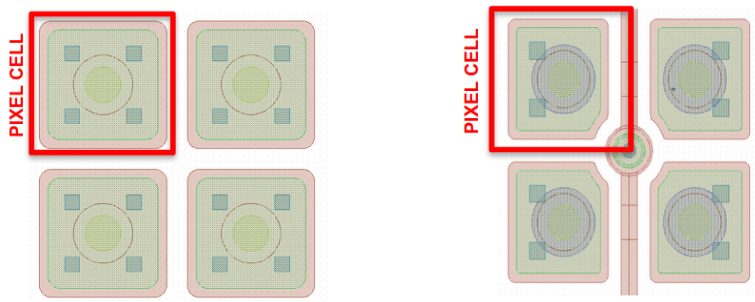


**(a)** No-PT module **(b)** PT-module

**Figure 4.** Schematic drawing of a $2 \times 2$ pixel grid of the tested planar modules.

### 3.1 Planar modules

One of the tested planar modules features a punch-through (PT) structure: in the following it will be referred as PT module, while the other one as no-PT module. In figure 4 schematic drawings of a $2 \times 2$ pixel grid are shown for both the PT and the no-PT modules. The thresholds of the planar pixel modules were tuned inside the cooling box, to an average pixel threshold $V_{\text{thr}}$ of about 1400 electrons for the no-PT module and 1200 electrons for the PT module. The tuning was made targeting low thresholds and noise, having at most 1% noisy pixel channels. The noisy pixels were masked offline during data analysis.

In figure 5, the global hit detection efficiency versus the applied bias voltage[2] $V_{\text{bias}}$ is shown, for perpendicular incident tracks. The hit detection efficiency of the DUT is calculated from the available trajectories with a hit in the timing reference module, and looking for a hit in the DUT. The no-PT module reaches an efficiency greater than 99% at a bias voltage of about 210 V. The leakage current in this module was 540 µA at 295 V, which is higher than expected and probably caused by a bad cooling contact between the copper bar and the DUT. The hit efficiency for the PT module starts saturating at around 200 V, and reaches a maximum value of 97.6% at 390 V. In this case the leakage current was 50 µA at 390 V.

In figure 6 the no-PT module hit efficiency maps for a $2 \times 2$ pixel grid are shown, for perpendicular tracks and for different bias voltages: the efficiency grows and gets more uniform by increasing the bias voltage. For low bias voltages, a small efficiency drop is visible at the intersection of four pixels. This effect is due to charge sharing between the four pixels and the charge trapping due to the irradiated silicon: hits in this region are more likely to be under-threshold and therefore not detected by the readout chip. By increasing the bias voltage, and hence the electric field, this effect is considerably mitigated.

In figure 7 the PT module hit efficiency maps for a $2 \times 2$ pixel grid are shown, for perpendicular tracks and for different bias voltages. In the punch-through implant region, the efficiency goes down to $\simeq$ 80–85%, but it recovers by increasing the bias voltage.

Rotations with respect to the beam axis are also extremely effective, as can be seen in the hit efficiency maps in figure 8. With a rotation by only 12°, the hit detection efficiency in the

[2]All the bias voltages shown in this paper are effective voltages, evaluated after having taken into account the voltage drop on the limiting resistors in series to the high voltage bias circuit.



2020 JINST 15 C02016

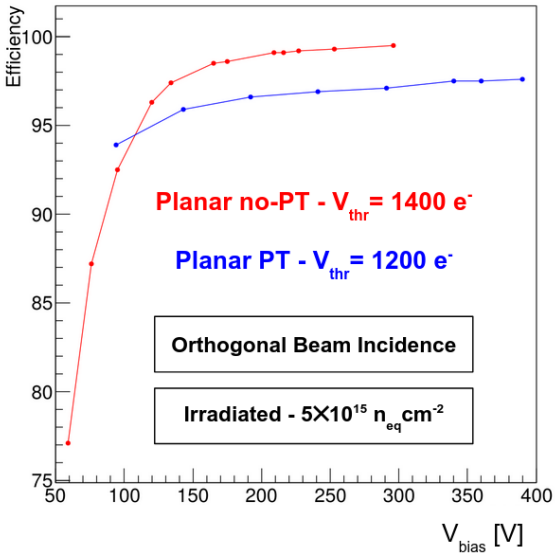


**Figure 5.** Planar modules' hit detection efficiency versus the applied bias voltage for orthogonal beam incidence.

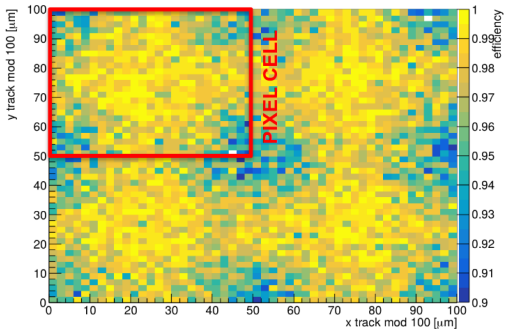


**(a)** $V_{\text{bias}} = 134\,\text{V}$

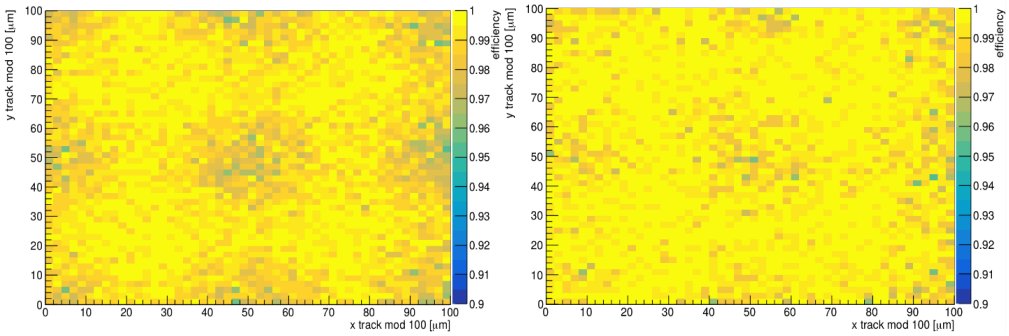


**(b)** $V_{\text{bias}} = 215\,\text{V}$ **(c)** $V_{\text{bias}} = 295\,\text{V}$

**Figure 6.** Planar no-PT module hit detection efficiency maps for a $2 \times 2$ pixel grid, for orthogonal beam incidence and for increasing values of the bias voltage. The efficiency colour scales are the same, and start at 90% efficiency.



2020 JINST 15 C02016

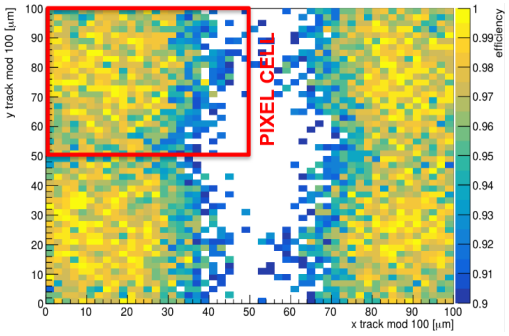


**(a)** $V_{\text{bias}} = 94$ V

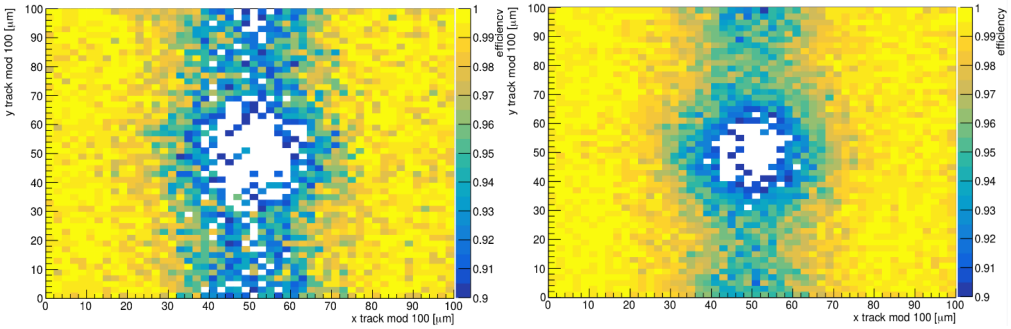


**(b)** $V_{\text{bias}} = 192$ V **(c)** $V_{\text{bias}} = 390$ V

**Figure 7.** Planar PT module hit detection efficiency maps for a 2×2 pixel grid, for orthogonal beam incidence and for increasing values of the bias voltage. The efficiency colour scales are the same, and start at 90% efficiency.

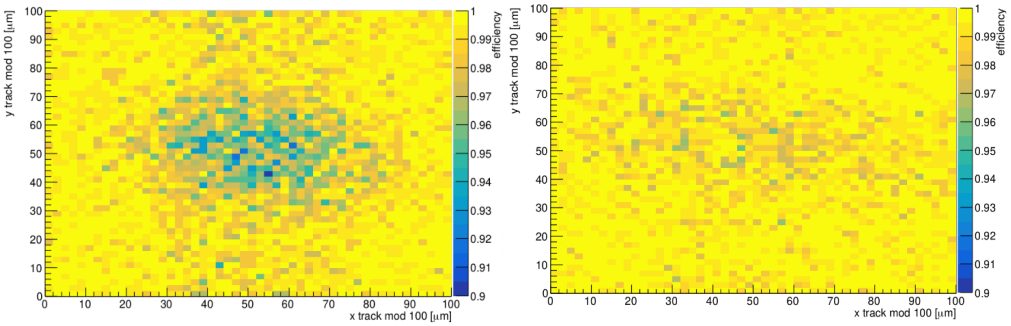


**(a)** $V_{\text{bias}} = 390$ V, Rotation angle = 12° **(b)** $V_{\text{bias}} = 390$ V, Rotation angle = 20°

**Figure 8.** Planar PT module hit detection efficiency maps for a 2 × 2 pixel grid, for different rotation angles. The efficiency colour scales are the same, and start at 90% efficiency.

punch-through implant region is greater than 90%, while at 20° the efficiency is almost uniform across the four pixels. The global efficiency is greater than 99% with a rotation by only 15°.

In the future CMS tracker, most of the tracks from the impact point will pass through the pixel modules with an angle greater than 15°, therefore the efficiency loss due to the punch-through structure would be extremely limited.



2020 JINST 15 C02016

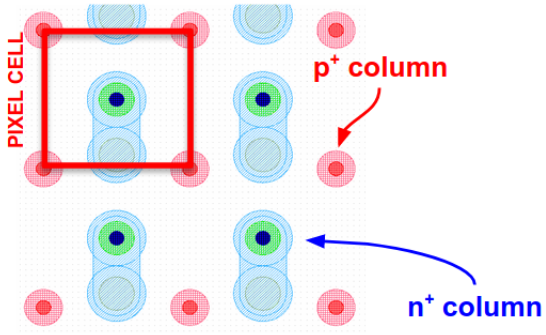


**Figure 9.** Schematic drawing of a $2 \times 2$ pixel grid of the tested 3D module.

### 3.2 3D Module

In figure 9 a schematic drawing of a $2 \times 2$ pixel grid of the tested 3D module is shown. The module was tuned inside the cooling box, to an average pixel threshold of about 1150 electrons. Also in this case, the tuning was made targeting low thresholds and noise, having at most 1% noisy pixel channels. The noisy pixels were masked offline during data analysis.

In figure 10, the global hit detection efficiency versus the applied bias voltage is shown, for perpendicular incident tracks. The hit efficiency starts saturating at around 110 V, and reaches a maximum value of 98.8% at 146 V. A rotation by 6° is enough to reach a hit efficiency greater than 99%. The leakage current was 100 µA at a bias voltage of 110 V.

This module was irradiated at the CERN PS: due to the limited beam dimensions, the irradiation was not uniform across the module. In figure 11 the hit efficiency map for the entire area of the Linear front-end is shown, for two different applied bias voltages: at 28 V the sensor is under-depleted and in the center of the front-end a large efficiency drop can be seen, corresponding to the most irradiated area. With a bias voltage of 146 V the sensor is over-depleted, and the efficiency is uniform across the Linear front-end, therefore the inefficiency in correspondence to the most irradiated area appears to be recovered. In order to verify this assumption, we divided the Linear front-end area into six smaller zones, and evaluated the hit efficiency on each of these smaller subsets of pixels. The results are compatible with the global efficiency (about 98.8%), therefore the hit detection efficiency is uniform across the whole Linear front-end, at least at high bias voltages.

In figure 12 the 3D module hit efficiency maps for a $2 \times 2$ pixel grid are shown, for perpendicular tracks and for different applied bias voltages. At low bias voltage, the efficiency is higher for hits near the $n^+$ columns, which are the collecting electrodes, because the drift path of the charge carriers is shorter, and they have a lower probability to get trapped in the silicon defects produced by irradiation. The efficiency becomes more uniform across the pixels by increasing the applied bias voltage.

We also took measurements at different DUT rotation angles with respect to the beam axis, in order to evaluate the pixel resolution as a function of the rotation. The DUT coordinates will be called rotated and non-rotated in the following.

For perpendicular incident tracks, the expected resolution is the trivial one:

$$\mathrm{res}_{\mathrm{trivial}} = 50/\sqrt{12}\,\mu\mathrm{m} \tag{3.1}$$



2020 JINST 15 C02016

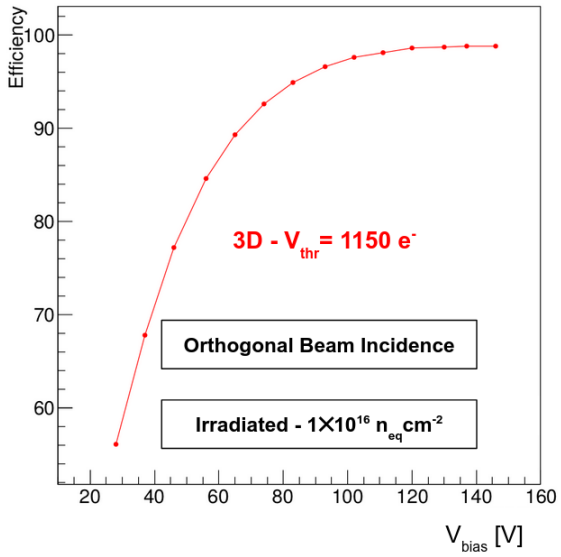


**Figure 10.** 3D module hit detection efficiency versus the applied bias voltage for orthogonal beam incidence.

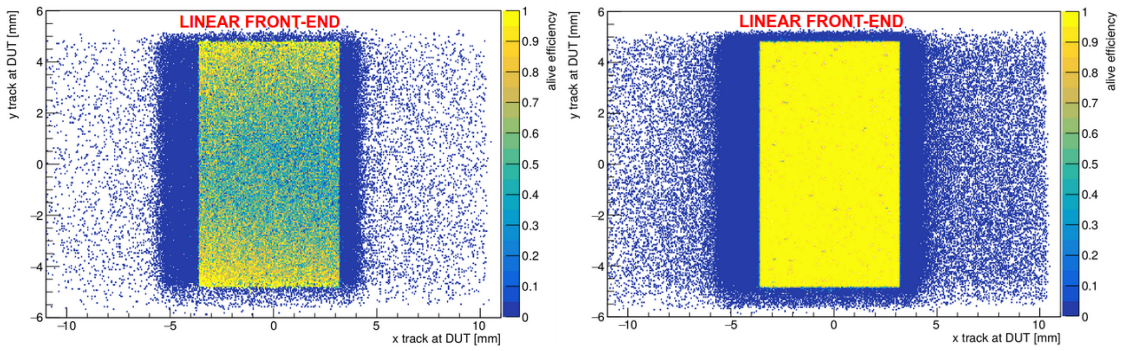


**(a)** $V_{\text{bias}} = 28\,\text{V}$ **(b)** $V_{\text{bias}} = 146\,\text{V}$

**Figure 11.** 3D module hit detection efficiency map over the whole Linear front-end, for increasing values of the applied bias voltage.

Fits were performed on the residual distributions of the two coordinates, using a student's $t$-distribution, which shows good accordance with the experimental data. Using the $\sigma$ from the fit for the non-rotated coordinate (for which we expect the trivial resolution) an estimation of the telescope resolution can be performed:

$$\text{res}_{\text{tele}} = \sqrt{\sigma^2_{\text{non-rot}} - \text{res}_{\text{trivial}}{}^2} \simeq 10\,\mu\text{m} \tag{3.2}$$

Then, the resolution for the rotated coordinate can be estimated with:

$$\text{res}_{\text{rot}} = \sqrt{\sigma^2_{\text{rot}} - \text{res}_{\text{tele}}{}^2} \tag{3.3}$$

In figure 13 the resolution versus the rotation angle is shown. The best resolution, about 5.7 µm, is achieved at $\simeq 20\,^\circ$. This is expected from the geometry of the pixel sensor, because tracks passing



2020 JINST 15 C02016

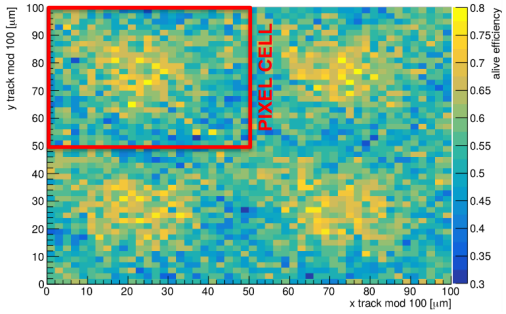


**(a)** $V_{\text{bias}} = 28\,\text{V}$

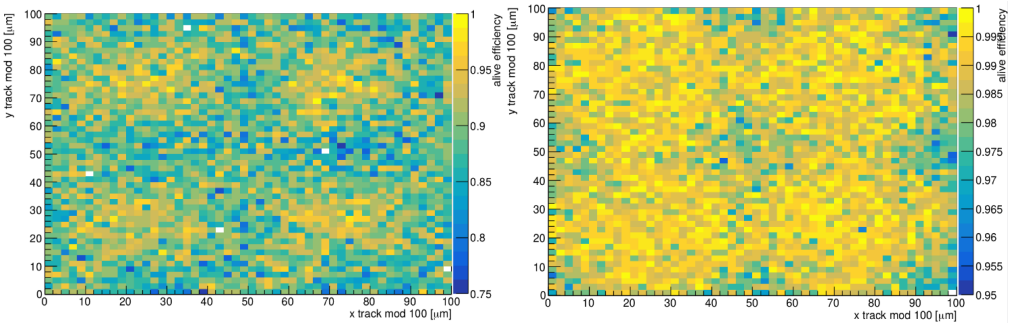


**(b)** $V_{\text{bias}} = 65\,\text{V}$ **(c)** $V_{\text{bias}} = 146\,\text{V}$

**Figure 12.** 3D module hit detection efficiency maps for a $2 \times 2$ pixel grid, for orthogonal beam incidence and for increasing values of the bias voltage. The efficiency colour scales are different.

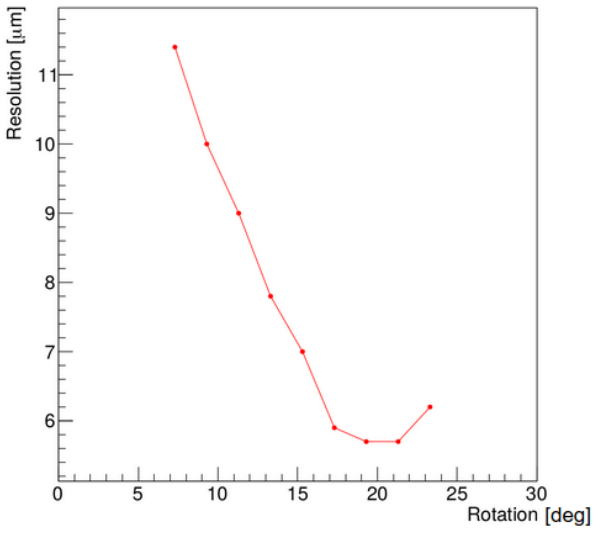


**Figure 13.** 3D module resolution versus the rotation angle with respect to the beam axis.

through the sensor with this angle always release charge in at least two pixels, which leads to a better resolution.

## 4 Conclusions

The upgrade of the CMS tracker for the HL-LHC will require radiation hard pixel sensors because of the expected extreme fluences.

We have obtained good results with the irradiated ($0.5 \times 10^{16}$ $n_{eq}/cm^2$) planar pixel modules, both with and without the punch-through structure, as they are fully efficient at an applied voltage of $\simeq$ 200 V. The inefficiency related to the punch-through structure is mitigated by rotation. The planar modules are already compliant with the radiation level expected in the second layer of future CMS tracker after 10 years of operations.

The irradiated ($1 \times 10^{16}$ $n_{eq}/cm^2$) 3D pixel module is also very good, as it is fully efficient at a bias voltage of 100 V. We obtained a resolution of 5.7 μm for a 20° rotation angle. The 3D module is already compliant with half the radiation level expected in the first layer of the future CMS tracker after 10 years of operations.

CMS is planning irradiations up to a fluence equivalent for the full HL-LHC lifetime radiation level of the innermost layer and test beam campaigns to verify the performances after such high fluences.


## Acknowledgments

We wish to thank Mirko Brianzi (INFN Firenze) for his invaluable help in the construction and wire-bonding of the pixel modules. We also wish to thank Daniel Pitzl and Aliakbar Ebrahimi for the constant support during the test beam. This work was supported by the H2020 project AIDA-2020, GA no. 654168.


## References


[1] CMS collaboration, *The Phase-2 Upgrade of the CMS Tracker*, CERN-LHCC-2017-009 (2017).

[2] G.F. Dalla Betta at al., *Small pitch 3D devices*, PoS(Vertex 2016)028.

[3] M. Garcia-Sciveres, *The RD53A Integrated Circuit*, CERN-RD53-PUB-17-001 (2017).

[4] H. Jansen, S. Spannagel, J. Behr, A. Bulgheroni, G. Claus, E. Corrin et al., *Performance of the EUDET-type beam telescopes*, *EPJ Tech. Instrum.* **3** (2016) 7.


2020 JINST 15 C02016